Immunospecific Targeting of CD45 Expressing Lymphoid Cells: Towards Improved Detection Agents of the Sentinel Lymph Node

Tianqing Liu [a], Aidan Cousins [a], Chia-Chi Chien [b], Ivan Kempson [b], Sarah Thompson [c], Yeukuang Hwu [b], Benjamin Thierry [a]*

a. Ian Wark Research Institute, University of South Australia, Mawson Lakes Campus, Mawson Lakes, Adelaide, SA 5095, Australia

b. Institute of Physics, Academia Sinica, Nankang, Taipei 115, Taiwan

c. Department of Surgery, University of Adelaide, Adelaide, SA 5000

Benjamin.Thierry@unisa.edu.au

Abstract

This study was designed to demonstrate the potential of small nanoparticulate lymphotropic contrast agents designed to bind with high affinity to lymphoid cells overexpressing the CD45 antigen. To this end, small gold nanoparticles used as model were conjugated to anti-CD 45 antibodies and injected in mice in the dorsal toe of the fore/hind paw. Chemical analysis demonstrated rapid uptake and transport of the nanoparticles in the lymphatic as well as significant retention of the nanoparticles with high binding affinity to lymphoid cells in the popliteal and axillary lymph nodes in comparison to non-targeted nanoparticles.

1. Introduction

Accurate staging of cancer is critical to predict overall prognosis as well as to decide on the most appropriate treatment(s), and to evaluate the tumour's response to those treatments. The role of lymph node metastasis has been well-demonstrated in the systemic dissemination of cancer, and therefore the lymph node status is of vital importance in the staging process [1; 2]. Current lymph node staging procedures are based on structural abnormalities (such as size and shape) and pathological examination of biopsies, guided or not by imaging-based detection of the sentinel lymph node(s) (SLNs). The SLN concept describes the preferential lymphatic metastasis of a primary tumour to one or more regional lymph nodes. Identification of the SLNs in current clinical practice is performed using dyes for direct intra-operative visualization and radiolabelled lymphotropic colloids coupled with nuclear imaging. When injected near the primary tumour, the imaging agent is taken up by the adjacent lymphatic and transported to the SLNs. In Australia for instance, the clinical lymphotropic radiotracer is ^{99m}Tc-antimony trisulfide [3]. For cancers where the lymphatic network is well mapped, such as breast cancer, biopsy-based assessment of SLN status is commonly used to minimize the burden of lymphadenectomy side-effects and associated morbidity. The relevance and utility of the SLN concept in other solid tumours such as gastrointestinal cancer has been more controversial with continued debate regarding its role, if any, in staging and treatment algorithms [4; 5]. The latter, however, is more the consequence of challenges associated with precise lymphatic mapping for such cancers rather than pathophysiological considerations. In the context of many deeply-situated cancers, current lymphoscintigraphy procedures are severely limited by the inherent low spatial resolution of nuclear imaging as well as by the "shine through effect" associated with the close proximity of SLNs to the primary tumour [6].

There is therefore a critical need to develop novel combinations of lymphotropic contrast agents and related imaging modalities [7]. Fostered by recent advances in nanotechnology, nanoparticle contrast agents are being actively developed and are now entering the clinical arena [8; 9]. In the context of lymphatic mapping, a range of novel nanoparticle contrast agents compatible with imaging modalities routinely used in the clinical practice have been developed, including iron oxide nanocrystals for magnetic resonance imaging [10], high atomic number nanoparticles (e.g. gold, bismuth, iodine) for CT imaging [11], nanobubbles and nanoemulsions for ultrasound imaging [12; 13], plasmonic nanoparticles for photoaccoustic imaging [14], and quantum dots for fluorescence-based imaging [15].

Although the behaviour of nanoparticle contrast agents within the lymphatics is directly correlated to their size and, to a lesser extent, their non-specific affinity for lymphatic tissues, the structure-activity relationship remains unclear. A general rule is that small molecules, such as those based on blue dyes, diffuse rapidly through the lymphatics and reach the SLNs within minutes. On the other hand, larger lymphotropic agents such as antimony-based radiocolloids are retained longer in the SLNs, which minimizes the risk of erroneous diagnosis but their slow diffusion rate often precludes intraoperative mapping of the SLNs. In an attempt to solve this dilemma, small lymphotropic agents designed to bind to macrophages and therefore to be retained in the lymph nodes are being developed. The most advanced of these next generation lymphotropic agents, Lymphoseek, is a ^{99m}Tc labelled dextran-mannose conjugate designed to have increased retention in the SLNs [16; 17]. Two Phase 3 multi-centre clinical trials have been completed and the U.S. Food and Drug Administration (FDA) has recently accepted a New Drug Application for this radiopharmaceutical. Although such agents are typically associated with faster clearance from the injection site when compared to relatively large colloid-based agents,

which could aid in reducing the "shine-through effect", they remain intrinsically limited by the poor spatial resolution of nuclear imaging. In addition, the very rapid transport of such agents to the SLNs makes it challenging to accurately image lymphatic drainage.

Based on the previous findings, we hypothesize here that nanoparticle contrast agents in the 10-30 nm size range with high binding affinity for lymphoid cells are ideal imaging agents of the SLNs. On one hand, their dynamic transport in the lymphatics can be readily controlled by tuning their hydrodynamic size. On the other hand, their binding affinity and consequently their retention in the lymph nodes can be controlled through bioconjugation with biologically active ligands. Molecularly targeted (herein collectively referred to as 'immunotargeted') nanoparticles are being actively developed towards increasing their therapeutic index and diagnostic utility [8; 18]. A recent study illustrated the potential of such agents using mannose-conjugated gold nanoparticles, which were found to accumulate in the popliteal lymph nodes after injection in rat's footpads [19].

The aim of this work was to investigate the lymphatic transport of small solid nanoparticles with high affinity for CD45 expressing cells. CD45 is a transmembrane glycoprotein of the leukocyte-specific receptor-like protein tyrosine phosphatase expressed at high density on nucleated haematopoietic cells. It is therefore a good molecular target candidate for delivery to lymphoid cells. 18 nm gold nanoparticles used here as a model for solid nanoparticle lymphotropic agents were conjugated with an anti-CD45 antibody, and their properties were characterized *in vitro* and *in vivo*. A critical requirement in the experimental design was avoiding aggregation during the bioconjugation procedure. This was achieved using a polymeric coating based on polyethylene glycol molecules (PEG) with different molecular weights designed to maximized bioconjugation yield while maintaining the colloidal stability of the nanoparticles. As a result of the high binding

affinity to CD45+ lymphoid cells, immunotargeted nanoparticles were retained in the popliteal and axillary lymph nodes after interstitial injection in mouse fore/hind paw while their non-conjugated counterparts were cleared from the lymphatics rapidly.

2. Materials and Methods

2.1. Materials

Chloroauric acid ($HAuCl_4 \cdot 3H_2O$), sodium citrate, N-hydroxysuccinimide (NHS), *N*-(3-Dimethylaminopropyl)-*N′*-ethylcarbodiimide hydrochloride (EDC), Phosphate Buffered Saline (PBS), and a silver enhancer kit were obtained from Sigma-Aldrich and used as received from the manufacturer without further purification. Water used in the experiments was purified with a Millipore water treatment system (organic content less than 5 ppb). Polyethylene glycol thiol (HS-PEG-COOH) with an average molecular weight of 5000 g/mol was purchased from Rapp polymer Gmbh. Short chain length PEG thiol acid (molecular weight 458.6) were purchased from Polypure. Mouse CD 45 (Ptprc monoclonal antibody) was purchased from Abnova.

2.2. Synthesis and Biofunctionalization of the Lymphotropic Agents

Gold nanoparticle synthesis and surface modification with PEG have been carried with minor modification from our previous study [20]. Briefly, citrate coated gold nanoparticles were prepared using the standard citrate method. Mixed thiolated PEG molecules comprising carboxylic functionalized short chain length PEG molecules (Fw 458.6) and PEG with longer chain length (Fw 5000) were used to stabilize the gold nanoparticles and enable optimal bioconjugation of monoclonal antibodies to the nanoparticles. The mixture of PEGs were prepared at a concentration of 1 mg/mL and mixed with a ratio of 4:1 (Fw 5000: Fw 458.6). The

mixed PEG solution was added to the gold nanoparticle solution under vortex and left to react for at least 6 hours at room temperature. After purification by centrifugation, the carboxyl groups on the PEGylated gold nanoparticles (1.0 mM, 1 mL) were activated using NHS (20 mg/mL) and EDC (15 mg/mL) for 5 min. The nanoparticle suspensions were then quickly centrifuged and resuspended into PBS (900 µL). Mouse anti-CD 45 antibody (0.5 mg/mL, 0.1 mL) was added rapidly to the activated gold nanoparticles and left to react at room temperature and stored at 4 ^{o}C after reaction. The antibody-conjugated nanoparticles were washed with PBS twice at 4 ^{o}C prior to use.

The physicochemical properties of the nanoparticles before and after the bioconjugation were determined using UV-Vis absorption and dynamic light scattering. UV-Vis spectra were determined using a Varian Cary 5 UV-Vis-NIR spectrophotometer at room temperature. The hydrodynamic diameter of gold nanoparticles was measured via dynamic light scattering using a Zetasizer Nano ZS equipped with a 633nm He-Ne laser (Malvern Instruments). The morphology and size distribution of gold nanoparticles prepared on a copper grid were analysed using a Philips CM100 transmission electron microscope (TEM).

2.3. Binding Affinity of the Anti-CD45 Bioconjugated Nanoparticles to Macrophages

To determine the active targeting effect of the immuno-functionalized gold nanoparticles, an *in vitro* assay was designed using RAW 264.7 macrophages used here as a model for lymphatic cells. RAW 264.7 macrophage cells were cultured in complete media consisting of Dulbecco's Modified Eagle's Medium supplemented with 10% (v/v) fetal bovine serum (FBS) in a humidified incubator at 37 ºC, 5% CO_2, and 100% humidity. A custom-made silicone well chamber device was cleaned and mounted on a clean glass coverslip. The glass surface was

treated with poly-L-lysine (1 mg/mL) before seeding the cells. Cells were plated into the wells at densities of 10,000-cells per well. After 24 h cell culture, the cells were incubated for 2 h at 37 °C with gold nanoparticles (0.01 mM and 0.04 mM Au concentration) conjugated or not with anti-CD45 antibody. Cells were then extensively washed in PBS and fixed in cold methanol at -20 °C. Triplicate samples were performed for each analysis and each test was repeated three times.

To enable microscopic visualization of cellular binding, gold nanoparticles were enlarged using standard silver-enhancement, washed thoroughly, and mounted in a mounting media for observation. The cellular binding of the targeted and non-targeted nanoparticles was visualized using a Nikon inverted light microscope operating in bright field under high magnification (100× objective, oil-immersion bright field condensers). The percentage of cells positive for gold nanoparticle binding (the number of gold nanoparticle targeted cells vs. total cells in the image) was determined by manual cell counting. The bright field microscopy study was complemented with reflectance confocal microscopy (LSM510) which provided higher imaging quality and increased sensitivity to the presence of the gold nanoparticles. In reflectance confocal microscopy, the high light scattering associated with plasmonic nanoparticles enable observations at the single nanoparticles level [21; 22]. To determine the three dimensional intracellular locations of the total NPs, vertical spatial images of nanoparticles within the RAW cells were generated by z-scans in 0.25 μm steps. The z-stack images were overlaid for each sample to confirm the targeting ability of different functionalized gold nanoparticles to cells.

2.4. Lymphatic Transport and Retention of the anti-CD45 Nanoparticles

BALB/cByJNarl mice (5–7 weeks old) were purchased from National Laboratory Animal Center (NLAC) in Taiwan and all procedures involving animals were approved by Academia Sinica Institutional Animal Care and Utilization Committee (ASIACUC). BALB/cByJNarl mice were anesthetized with isofluorane and injected subcutaneously in the dorsal toe of the fore/hind paw with PEGylated gold nanoparticles and anti-CD45 gold nanoparticles (9 mice per group) at a gold dose of 1 mg/kg body weight (Au concentration of 1 mg/mL). Mice were euthanized 2, 6 and 24 h post-administration of the gold nanoparticles. The axillary and popliteal lymph nodes were collected, cleaned and weighed for the lymphatic distribution of the particles with different surface functionalization. For ICP-MS analysis, the lymph nodes with the gold nanoparticles were dissolved by aqua regia (the volume ratio of 37% HCl and 70% HNO_3 was 3:1). The total amount of gold in harvested lymph nodes after nanoparticle treatment was quantified by ICP-MS (ICP-MS 7500 CS, Agilent Technologies, USA).

3. Results and discussion

3.1. Design of the Bioconjugated Contrast Agents

Gold nanoparticles were chosen here as a model nanoparticle contrast agent owing to the existence of well-established synthesis routes with excellent control of the particle size as well as their unique optical properties [23]. Nanoparticles with an average diameter of 18 nm were synthesized and the size was confirmed by TEM measurement (Figure 2. A). Previous studies have shown that nanoparticles within this size-range transport rapidly in the lymphatics [24; 25; 26], making them ideal for this study.

PEGylated gold nanoparticles were engineered with an optimized coating procedure designed to prevent aggregation of the nanoparticles while enabling high conjugation yields with biological

ligands. The terminal carboxylic acids of PEG molecules on the gold nanoparticles were conjugated to anti-CD45 antibodies via carbodiimide chemistry. The colloidal stability of the as-synthesized gold nanoparticles and the functionalized gold nanoparticles was established by dynamic light scattering and UV-Vis measurements. The hydrodynamic radius increased by 15 nm after bioconjugation with anti-CD45 antibodies, which confirmed the successful surface modification of nanoparticles (Figure 2. B). The monomodal distribution of the gold nanoparticles before and after bioconjugation showed that particles were well dispersed and aggregation-free. The latter was confirmed by UV-Vis absorption, where no broadening of the plasmon bands could be observed for bioconjugated nanoparticles (Figure 2. C). Nanoparticles are prone to aggregation during bioconjugation with biological ligands and it is critical to determine the hydrodynamic size distribution of bioconjugated nanoparticles prior to their application in biological systems [27; 28]. In the present study, aggregation would have drastically influenced the lymphatic transport of the nanoparticles and in turn have prevented meaningful comparison between the bioconjugated and non-conjugated contrast agents.

3.2. *In vitro* Binding Affinity of the anti-CD45 Nanoparticles to Lymphatic Cells

To compare the *in vitro* cellular binding of the nanoparticles targeted or not to CD45+ cells, these two groups of nanoparticles were incubated with macrophages for 2 h at a relatively low concentration of gold nanoparticles (0.01 mM and 0.04 mM) chossen to avoid binding-saturation. The murine RAW 264.7 macrophage cell line was selected as an *in vitro* model of lymphoid cells. Taking advantage of the high Rayleigh scattering of gold nanoparticles after silver enhancement, light microscopy was used to determine the percentages of RAW 264.7 cells displaying unambiguous positive labelling with the nanoparticles. As shown in Figure 3, anti-

CD45 conjugated nanoparticles had a high binding affinity to the macrophages as demonstrated by the fact that all tested cells were successfully targeted by the nanoparticles. On the other hand, only minimal binding was observed for the non-targeted nanoparticles as less than 10% of the cells showed unambiguous staining by the nanoparticles (Figure 3. C). To obtain further insight into the cell-nanoparticle interactions, the cells were imaged by confocal microscopy in the reflectance mode. Scattering of incident light dominates over plasmon absorption for plasmonic nanoparticles larger than approximately 40 nm, which enable their visualization at the single nanoparticle level in the reflectance mode [21; 22; 29]. Figure 4 shows the phase contrast and reflectance images for the RAW cells after incubation with the nanoparticles for 2 hours and silver enhancement which was used to accentuate the scattering of the small nanoparticles used in this study. In order to represent the total amount of nanoparticles bound to or internalized inside the RAW 264.7 macrophages, z-stack data was overlaid to obtain an accurate rendering of nanoparticle-cell interactions. In agreement with previous reports, reflectance confocal imaging provided significantly increased sensitivity to the presence of the scattering nanoparticles in comparison to bright field and dark field microscopy. Reflectance data confirmed the bright field microscopy observations that the anti-CD45 conjugated nanoparticles have a very high binding affinity to the RAW 264.7 cells as shown by the very high staining rate observed after two hours (Figure 4. A-C). In contrast, negligible uptake of non-targeted PEGylated nanoparticles by the macrophages was observed in the confocal microscopic images (Figure 4. D-F). Even at very low concentration, the anti-CD45 targeted nanoparticles were taken up avidly by the macrophages (Figure 4. G-I). The presence of larger and bright structures in the reflectance images could be associated with endocytotic internalization of the nanoparticles after binding to the macrophages [30]. These *in vitro* studies confirmed that the PEG coating drastically inhibited

non-specific binding to macrophages while enabling efficient bioconjugation with biological ligands. The protective effect against phagocytosis of PEG-based nanoparticles coating originates in reduction of protein fouling and is strongly dependant on the properties of the polymeric adlayers [31].

3.3. Lymphatic Drainage and Retention in Mice

To investigate the lymphatic drainage of the nanoparticles conjugated or not with the anti-CD45 antibodies, BALB/cByJNarl mice were injected subcutaneously in the dorsal toe of the fore/hind paw (1 mg Au / kg body weight). At various time points, the animals were sacrificed and the axillary and popliteal lymph nodes were collected and analysed using ICP-MS to determine the gold concentration. Although the drainage distribution varies between individual mice, the injection through the hind pad typically drains to the popliteal (then on to iliac) [32]. The axillary lymph node serves as the first lymph node to receive the drainage from the fore pad.

Accumulation of the gold nanoparticles within the nodes could be readily visualized from the reddish colourization of the nodes (Figure 5.), which greatly facilitated the localization of the otherwise transparent nodes. Stronger colourization was typically observed for explanted lymph nodes in the anti-CD45 groups in comparison to the nodes from animals injected with non-targeted nanoparticles (Figure 5. B and C). The improved *in vivo* uptake and retention of the anti-CD45 nanoparticles was confirmed using ICP-MS. The time points chosen to quantify the dynamic lymphatic drainage were 2, 6, and 24 h post-injection (Figure 6.). At 2 h post injection, similar concentrations of gold were found in nodes for both the anti-CD45 targeted group and the non-targeted control (128 ng vs. 103 ng means for the anti-CD45 nanoparticles and control respectively, $p>0.05$). This result demonstrates that both nanoparticle preparations were rapidly

transported to the lymph nodes, in agreement with previous reports on the lymphatic uptake of nanoparticles in this size range [24; 25; 26]. The amount of gold in the lymph nodes was however significantly higher for subsequent time-points for animals administrated with anti-CD45 conjugated nanoparticles in comparison to the non-conjugated controls. Whilst the gold concentrations within the popliteal and axillary nodes fell below the limit of detection of the ICPMS at 6 and 24 hours for the control group, gold concentrations in the anti-CD45 targeted group increased after the 2 h time point. The peak accumulation time point for the popliteal lymph nodes was at 6 h (570 ng, 2.9 % ID at 6 h vs. 327 ng, 1.6 % at 24 h), whilst the amount of the immunotargeted nanoparticles continued to increase after 6 h until 24 h for axillary lymph nodes (182 ng, 0.9 % ID at 6 h vs. 470 ng, 2.4 % at 24 h). The ICPMS data demonstrates that the anti-CD45 conjugated nanoparticles were retained in the lymph nodes, most likely due to specific binding to CD45+ lymphoid cells which highly express the CD45 antigen. On the contrary, PEGylated controls were quickly cleared from the lymph nodes (within 6) and hence they had a much shorter retention time in the lymph nodes. These results can be compared qualitatively to those reported with Lymphoseek and other mannose-targeted lymphotropic agents. In a recent clinical study, the mean sentinel lymph node retention for Lymphoseek was 1.5±1.7% [33]. Similarly, 1.32 % of gold nanoparticles conjugated with mannose were retained in the popliteal nodes after injection in Wistar rats [19]. Although further studies are required, these data suggest that lymphotropic nanoparticulate contrast agents designed to bind with high affinity to lymphoid cells which intrinsically overexpress the CD45 antigen is a promising alternative to mannose-based targeting approaches. The high node retention observed in this study with anti-CD45 targeted nanoparticles was consistent to that obtained using anti-CD4 conjugated nanoparticles [28]. However, large aggregates (up to 500 nm) were found after the

antibody conjugation in these studies and the size variation upon bioconjugation make it difficult to draw conclusions on transport via the lymphatic drainage [27; 28]. To unravel the complex lymphatic behaviour of exogenous contrast agents, it is critical to fully characterize their physicochemical properties and control their interactions with biological components. The latter was achieved here by using mixed PEG coatings which enabled efficient bioconjugation with monoclonal antibodies while providing excellent colloidal stability during the conjugation process and in biological environments. In addition to their protective effect against nanoparticle aggregation, PEG-based nanoparticle coatings were found to drastically increase the lymphatic drainage of phospholipid liposomes [34]. The specific effect of the PEG coating could not be tested here, since nanoparticles without PEG coating rapidly aggregated during the conjugation as well as in biological environments, which precluded meaningful investigation of the chemistry versus size effects on nanoparticle lymphatic transport.

4. Conclusions

The metastatic status of regional lymph nodes is the most significant prognostic factor in breast cancer, melanoma and other solid tumors with lymphatic spread. Clinical application of the Sentinel Lymph Node concept remains limited in a number of diseases due to the limitations of the current lymphotropic tracers used to identify lymphatic drainage from the primary tumor. This study aimed to demonstrate the potential of lymphotropic nanoparticle contrast agents designed to bind with high affinity to lymphoid cells overexpressing the CD45 antigen. To this end, gold nanoparticles with a 18 nm diameter were prepared and bioconjugated with anti-CD45 antibodies through an optimized polyethylene glycol (PEG) coating designed to protect the nanoparticles from aggregation. Using a murine macrophage cell line as a model, the high

binding affinity for lymphoid cells of the anti-CD45 nanoparticles was demonstrated *in vitro*. In contrast, unconjugated nanoparticles showed minimal non-specific binding to the macrophage thanks to the dense PEG coating. Chemical analysis of the popliteal and axillary lymph nodes of mice was conducted at different time points after subcutaneous injection of the nanoparticles in the dorsal toe of the fore/hind paw. This study confirmed the rapid lymphatic uptake and transport of the small nanoparticles. At 6 and 24 hours, the anti-CD45 targeted nanoparticles were significantly retained in the nodes and compared favourably with lymphatic tracers targeting mannose receptors. The combination of small hydrodynamic size, optimal PEG coating and high binding affinity to CD45 positive lymphoid cells appears to be suitable for the development of advanced detection agents for the SLNs. Building on this study and the availability of advanced nanoparticulates contrast agents compatible with state-of-the-art imaging modalities such as magnetic resonance imaging, we expect that improved imaging procedures for pre- and intra-operative detection of the SLNs can be developed.

Conflict of interest

We here state that we did not have any conflict of interest for this paper.

Acknowledgements

This work was supported by the NSW Cancer Council and the International Synchrotron Access Program from the Australian Synchrotron. B. Thierry is supported by a NH&MRC CDA. The authors would like to thank Prof. Cory Xian for providing RAW cells and the Australian National Fabrication Facility (ANFF).

References

[1]K. Kawada, M.M. Taketo, Significance and mechanism of lymph node metastasis in cancer progression. Cancer Res. 71 (2011) 1214-1218.

[2]A.C.J. van Akkooi, C. Verhoef, A.M.M. Eggermont, Importance of tumor load in the sentinel node in melanoma: clinical dilemmas. Nat. Rev. Clin. Oncol. 7 (2010) 446-454.

[3]C. Tsopelas, Particle Size Analysis of 99mTc-Labeled and Unlabeled Antimony Trisulfide and Rhenium Sulfide Colloids Intended for Lymphoscintigraphic Application. J. Nucl. Med. 42 (2001) 460-466.

[4]Z. Wang, Z.-Y. Dong, J.-Q. Chen, J.-L. Liu, Diagnostic value of sentinel lymph node biopsy in gastric cancer: a meta-analysis. Ann. Surg. Oncol. 1-10.

[5]S. Thompson, D. Bartholomeusz, G. Jamieson, Sentinel lymph node biopsy in esophageal cancer: should it be standard of care? J. Gastrointest. Surg. 15 (2011) 1762-1768.

[6]C. van de Ven, P. De Leyn, W. Coosemans, D. Van Raemdonck, T. Lerut, Three-field lymphadenectomy and pattern of lymph node spread in T3 adenocarcinoma of the distal esophagus and the gastro-esophageal junction. Eur. J. Cardiothorac. Surg. 15 (1999) 769-773.

[7]R.Z. Karim, R.A. Scolyer, W. Li, V.S.K. Yee, J.G. McKinnon, L.-X.L. Li, R.F. Uren, S. Lam, A. Beavis, M. Dawson, P. Doble, D.S.B. Hoon, J.F. Thompson, False negative sentinel lymph node biopsies in melanoma may result from deficiencies in nuclear medicine, surgery, or pathology. Ann. Surg. 247 (2008) 1003-1010

[8]R. Weissleder, M.J. Pittet, Imaging in the era of molecular oncology. Nature 452 (2008) 580-589.

[9]H.S. Choi, J.V. Frangioni, Nanoparticles for biomedical imaging: fundamentals of clinical translation. Mol. Imaging. 9 (2010) 291-310.

[10]M.G. Harisinghani, J. Barentsz, P.F. Hahn, W.M. Deserno, S. Tabatabaei, C.H. van de Kaa, J. de la Rosette, R. Weissleder, Noninvasive detection of clinically occult lymph-node metastases in prostate cancer. N. Engl. J. Med. 348 (2003) 2491-2499.

[11]O. Rabin, J.M. Perez, J. Grimm, G. Wojtkiewicz, R. Weissleder, An X-ray computed tomography imaging agent based on long-circulating bismuth sulphide nanoparticles. Nat. Mater. 5 (2006) 118-122.

[12]P.A. Dayton, J.J. Rychak, Molecular ultrasound imaging using microbubble contrast agents. Front. Biosci. 12 (2007) 5124-5142.

[13]M. Hahn, A. Singh, P. Sharma, S. Brown, B. Moudgil, Nanoparticles as contrast agents for in-vivo bioimaging: current status and future perspectives. Anal. Bioanal. Chem. 399 (2011) 3-27.

[14]D. Pan, M. Pramanik, A. Senpan, S. Ghosh, S.A. Wickline, L.V. Wang, G.M. Lanza, Near infrared photoacoustic detection of sentinel lymph nodes with gold nanobeacons. Biomaterials 31 (2010) 4088-4093.

[15]E. Tanaka, H. Choi, H. Fujii, M. Bawendi, J. Frangioni, Image-guided oncologic surgery using invisible light: completed pre-clinical development for sentinel lymph node mapping. Ann. Surg. Oncol. 13 (2006) 1671-1681.

[16]S. Leong, J. Kim, M. Ross, M. Faries, C. Scoggins, W. Rich Metz, F. Cope, R. Orahood, A phase 2 study of (99m)Tc-tilmanocept in the detection of sentinel lymph nodes in melanoma and breast cancer. Ann. Surg. Oncol. 18 (2011) 961-969.

[17]A. Wallace, C. Hoh, S. Ellner, D. Darrah, G. Schulteis, D. Vera, Lymphoseek: a molecular imaging agent for melanoma sentinel lymph node mapping. Ann. Surg. Oncol. 14 (2007) 913-921.
[18]M.A. Phillips, M.L. Gran, N.A. Peppas, Targeted nanodelivery of drugs and diagnostics. Nano Today 5 (2010) 143-159.
[19]B.E. Ocampo-García, F.d.M. Ramírez, G. Ferro-Flores, L.M. De León-Rodríguez, C.L. Santos-Cuevas, E. Morales-Avila, C.A. de Murphy, M. Pedraza-López, L.A. Medina, M.A. Camacho-López, 99mTc-labelled gold nanoparticles capped with HYNIC-peptide/mannose for sentinel lymph node detection. Nucl. Med. Biol. 38 (2011) 1-11.
[20]B. Thierry, H.J. Griesser, Dense PEG layers for efficient immunotargeting of nanoparticles to cancer cells. J. Mater. Chem. 22 (2012) 8810-8819.
[21]S. Klein, S. Petersen, U. Taylor, D. Rath, S. Barcikowski, Quantitative visualization of colloidal and intracellular gold nanoparticles by confocal microscopy. J. Biomed. Opt. 15 (2010) 036015.
[22]U. Taylor, S. Klein, S. Petersen, W. Kues, S. Barcikowski, D. Rath, Nonendosomal cellular uptake of ligand-free, positively charged gold nanoparticles. Cytometry Part A 77A (2010) 439-446.
[23]D. Pissuwan, T. Niidome, M.B. Cortie, The forthcoming applications of gold nanoparticles in drug and gene delivery systems. J. Control Release. 149 (2011) 65-71.
[24]S.T. Reddy, A. Rehor, H.G. Schmoekel, J.A. Hubbell, M.A. Swartz, In vivo targeting of dendritic cells in lymph nodes with poly(propylene sulfide) nanoparticles. J. Control Release. 112 (2006) 26-34.
[25]R.-C. Ji, Lymphatic endothelial cells, tumor lymphangiogenesis and metastasis: New insights into intratumoral and peritumoral lymphatics. Cancer Metastasis Rev. 25 (2006) 677-694.
[26]M.A. Swartz, J.A. Hubbell, S.T. Reddy, Lymphatic drainage function and its immunological implications: From dendritic cell homing to vaccine design. Semin. Immunol. 20 (2008) 147-156.
[27]W. Eck, G. Craig, A. Sigdel, G. Ritter, L.J. Old, L. Tang, M.F. Brennan, P.J. Allen, M.D. Mason, PEGylated gold nanoparticles conjugated to monoclonal F19 antibodies as targeted labeling agents for human pancreatic carcinoma tissue. ACS Nano 2 (2008) 2263-2272.
[28]W. Eck, A.I. Nicholson, H. Zentgraf, W. Semmler, S.n. Bartling, Anti-CD4-targeted gold nanoparticles induce specific contrast enhancement of peripheral lymph nodes in X-ray computed tomography of live mice. Nano Lett. 10 (2010) 2318-2322.
[29]S.-W. Tsai, Y.-Y. Chen, J.-W. Liaw, Compound cellular imaging of laser scanning confocal microscopy by using gold nanoparticles and dyes. Sensors 8 (2008) 2306-2316.
[30]S.-H. Wang, C.-W. Lee, A. Chiou, P.-K. Wei, Size-dependent endocytosis of gold nanoparticles studied by three-dimensional mapping of plasmonic scattering images. J. Nanobiotechnology. 8 (2010) 33.
[31]C.D. Walkey, J.B. Olsen, H. Guo, A. Emili, W.C.W. Chan, Nanoparticle size and surface chemistry determine serum protein adsorption and macrophage uptake. J. Am. Chem. Soc. 134 (2011) 2139-2147.
[32]M.I. Harrell, B.M. Iritani, A. Ruddell, Lymph node mapping in the mouse. J. Immunol. Methods. 332 (2008) 170-174.

[33]A.M. Wallace, C.K. Hoh, K.K. Limmer, D.D. Darrah, G. Schulteis, D.R. Vera, Sentinel lymph node accumulation of Lymphoseek and Tc-99m-sulfur colloid using a “2-day” protocol. Nucl. Med. Biol. 36 (2009) 687-692.
[34]S.M. Moghimi, The effect of methoxy-PEG chain length and molecular architecture on lymph node targeting of immuno-PEG liposomes. Biomaterials 27 (2006) 136-144.

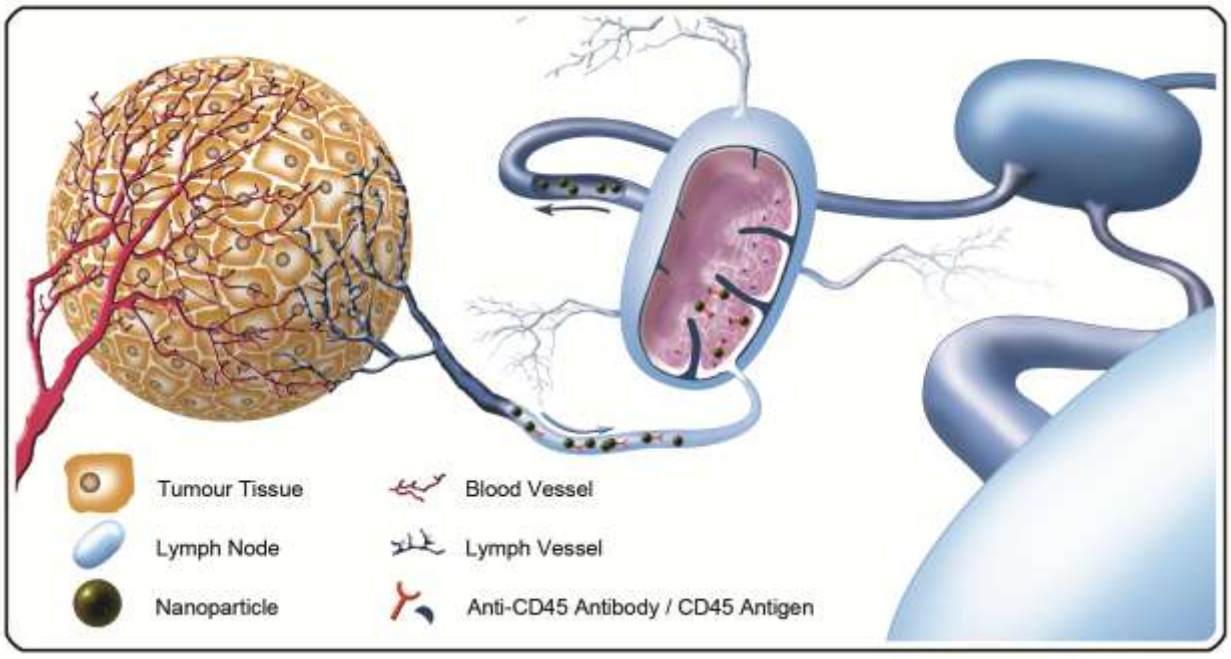

Figure 1. Schematic illustration of lymphatic drainage/retention of lymphotropic nanoparticulate tracers from the primary tumor in SLN imaging. Small nanoparticles are rapidly uptake and transported through the lymphatic and transit through the lymph nodes. Nanoparticles with high binding affinity with CD45 expressing lymphoid cells are retained in the nodes while non-targeted agents are cleared rapidly.

A

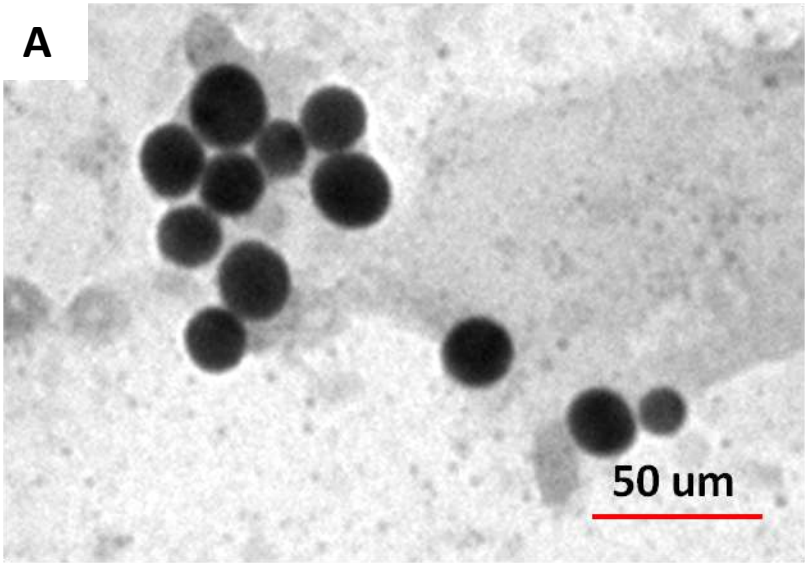
50 um

B

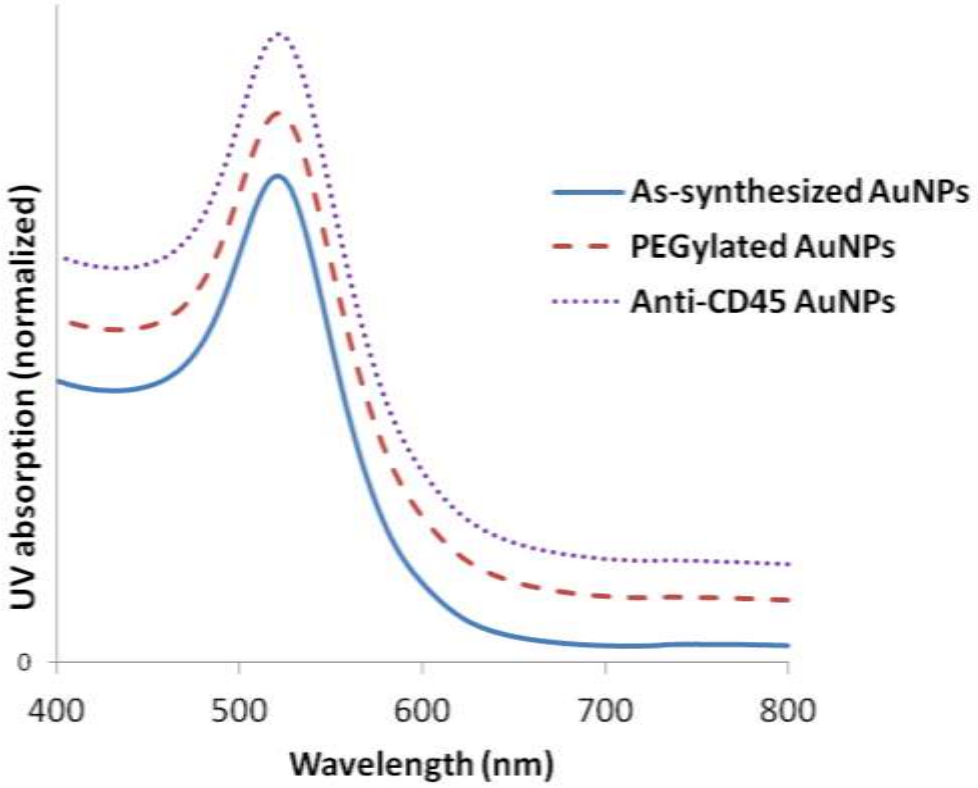
As-synthesized AuNPs
PEGylated AuNPs
Anti-CD45 AuNPs
UV absorption (normalized)
0
400
500
600
700
800
Wavelength (nm)

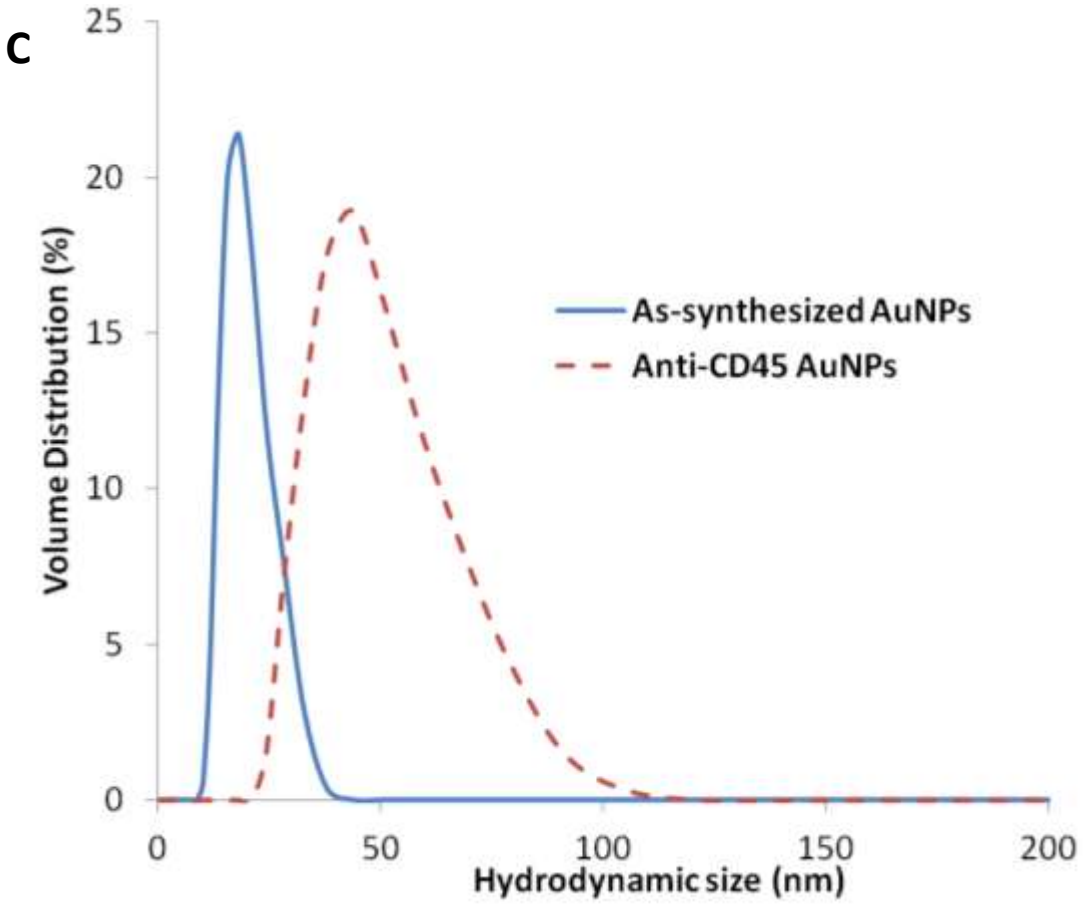

Figure 2. Characterization of gold nanoprobes. (A) A TEM image of the as-synthesized NPs; (B) UV-visible absorption of the as-synthesized, PEGylated, and anti-CD45 conjugated gold nanoparticles; (C) Hydrodynamic particle sizes of the as-synthesized and anti-CD45 conjugated gold nanoparticles.

A

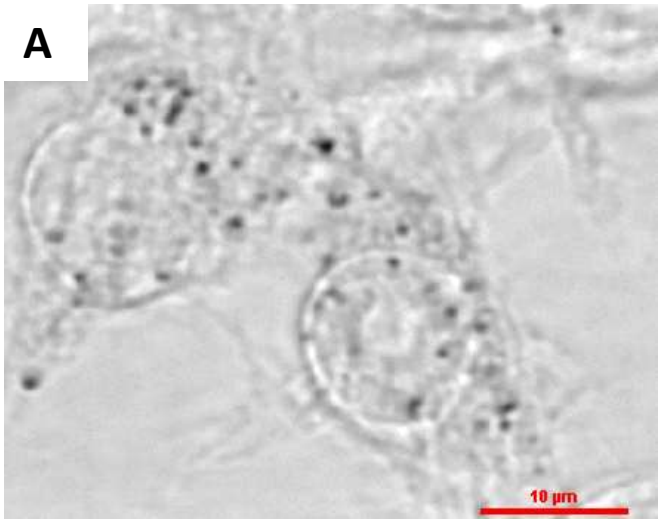

B

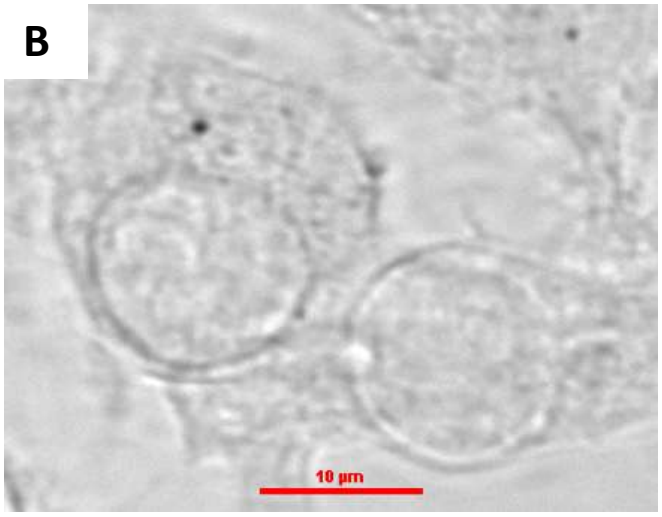

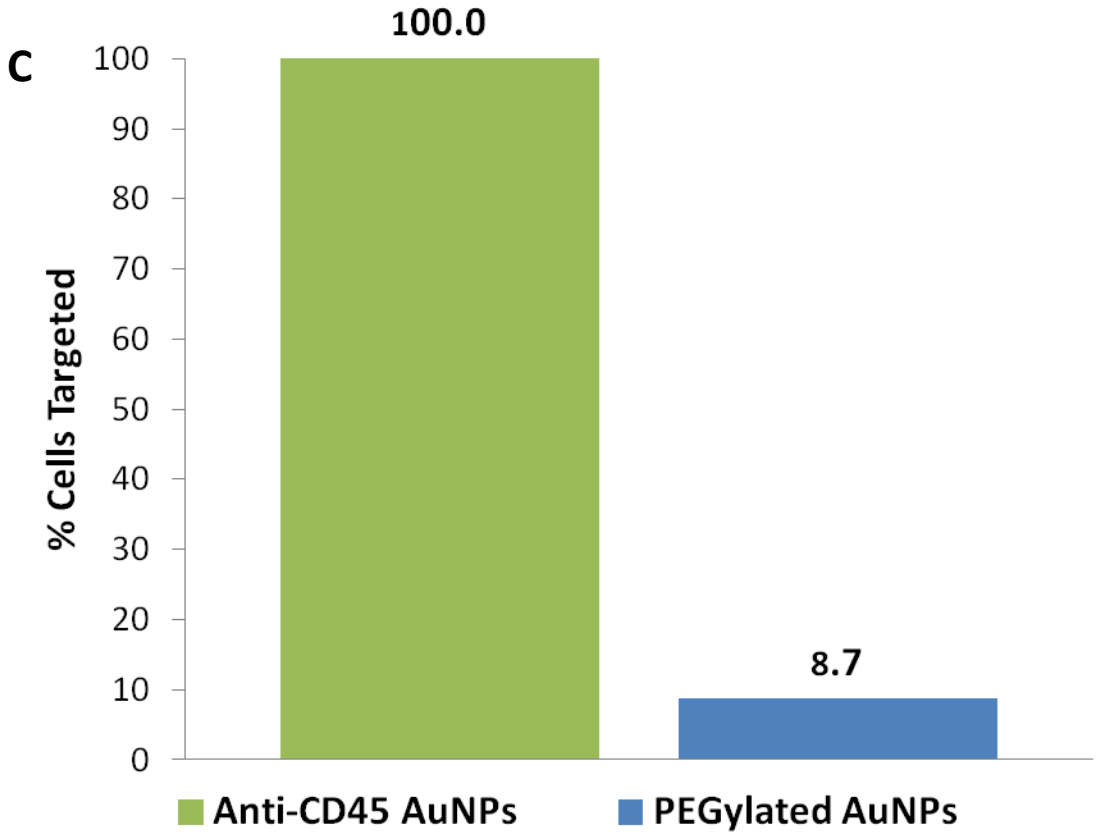

Figure 3. Bright field microscopic images of nanoparticles associated with RAW cells. (A) Anti-CD45 conjugated gold nanoparticles; (B) PEGylated gold nanoparticles; (C) Percentage of cells associated with anti-CD45 conjugated gold nanoparticles and PEGylated gold nanoparticles from 10 different images captured by light microscopy.

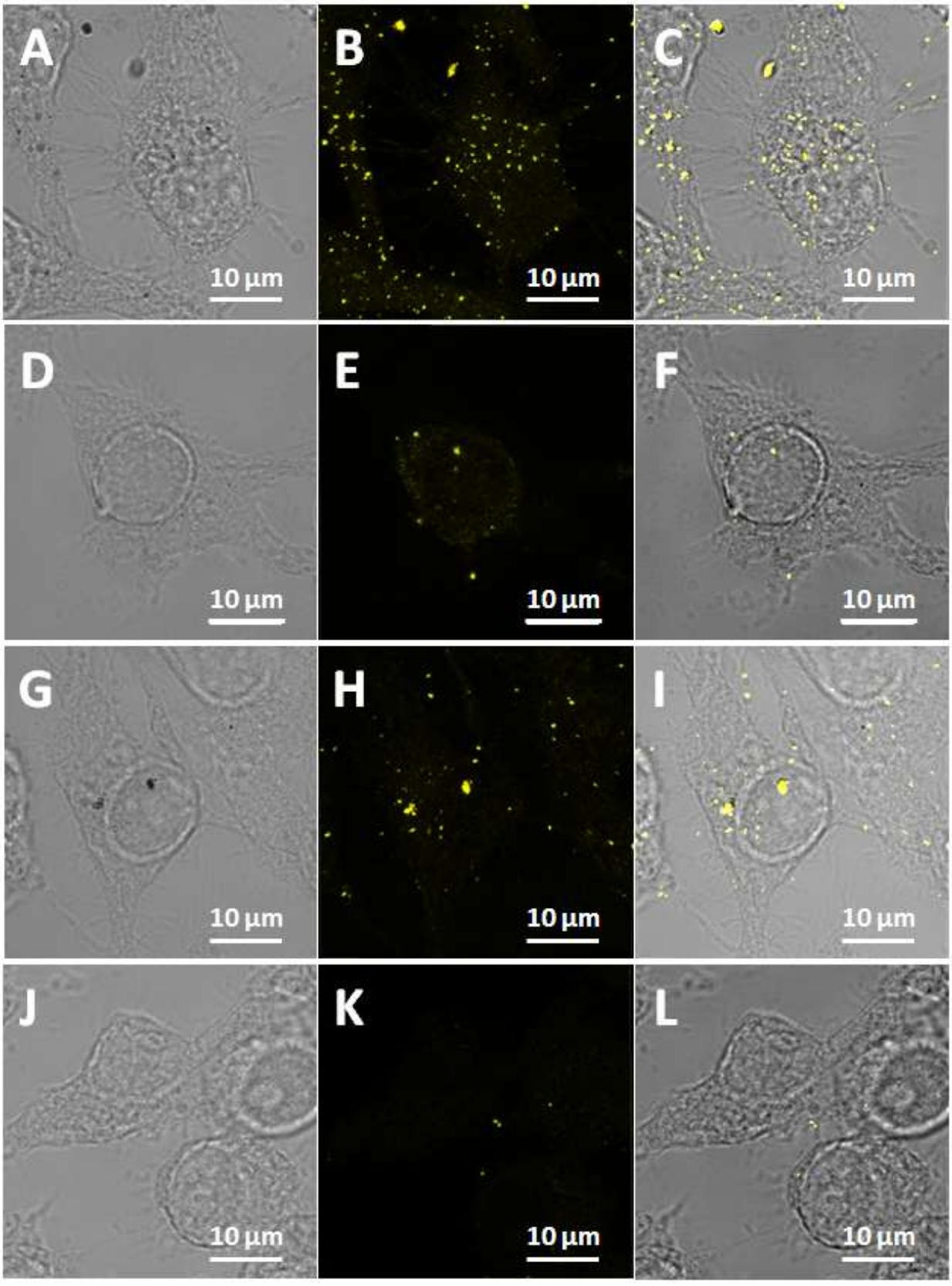
A
10 µm
B
10 µm
C
10 µm
D
10 µm
E
10 µm
F
10 µm
G
10 µm
H
10 µm
I
10 µm
J
10 µm
K
10 µm
L
10 µm

Figure 4. Confocal microscopic images (bright field, reflectance and their overlay) of nanoparticles binding to RAW cells. (A-C) Anti-CD45 conjugated gold nanoparticles at a gold concentration of 0.04 mM; (D-F) PEGylated gold nanoparticles at a gold concentration of 0.04 mM; (G-I) Anti-CD45 conjugated gold nanoparticles at a gold concentration of 0.01 mM; (J-L) PEGylated gold nanoparticles at a gold concentration of 0.01 mM.

Figure 5. Photographs showing nanoparticles. (A) Accumulation in the popliteal lymph node in a mouse before dissection 24 h post-injection; (B) Accumulation in the axillary lymph node excised and embedded in resin 24 h after anti-CD45 conjugated gold nanoparticles injection; (C)

accumulation in the axillary lymph node embedded in resin 24 h after PEGylated gold nanoparticle injection.

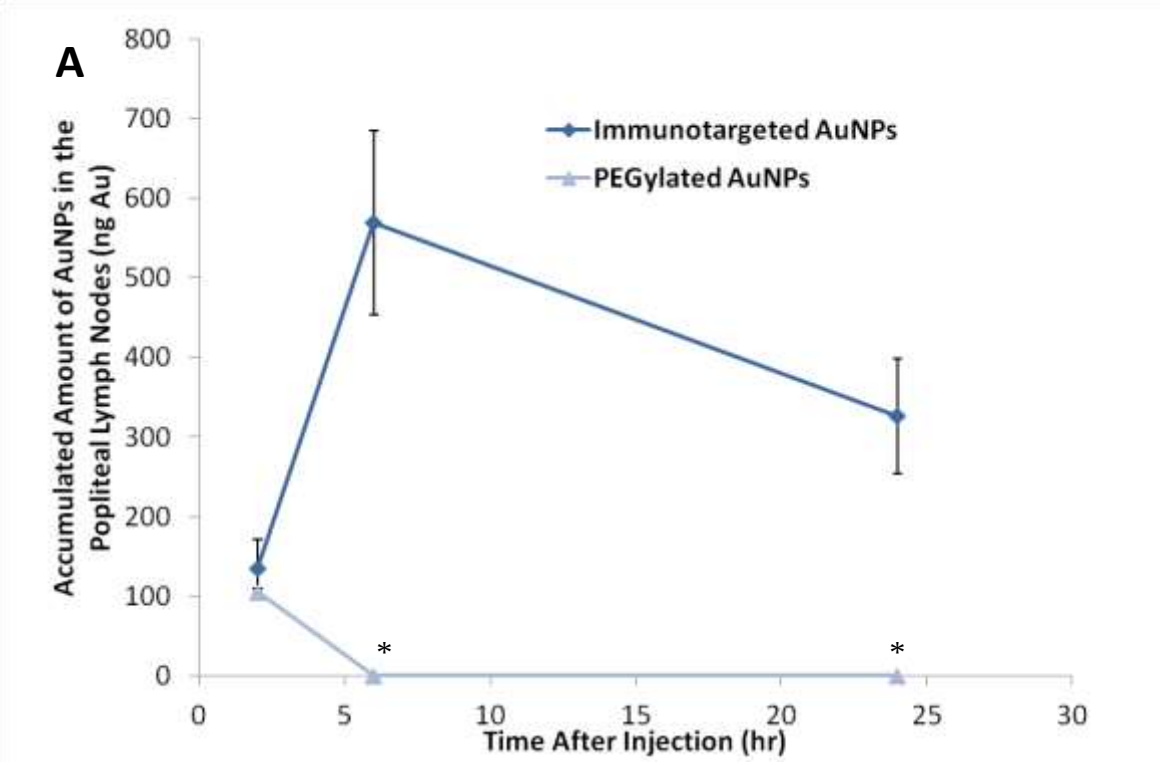

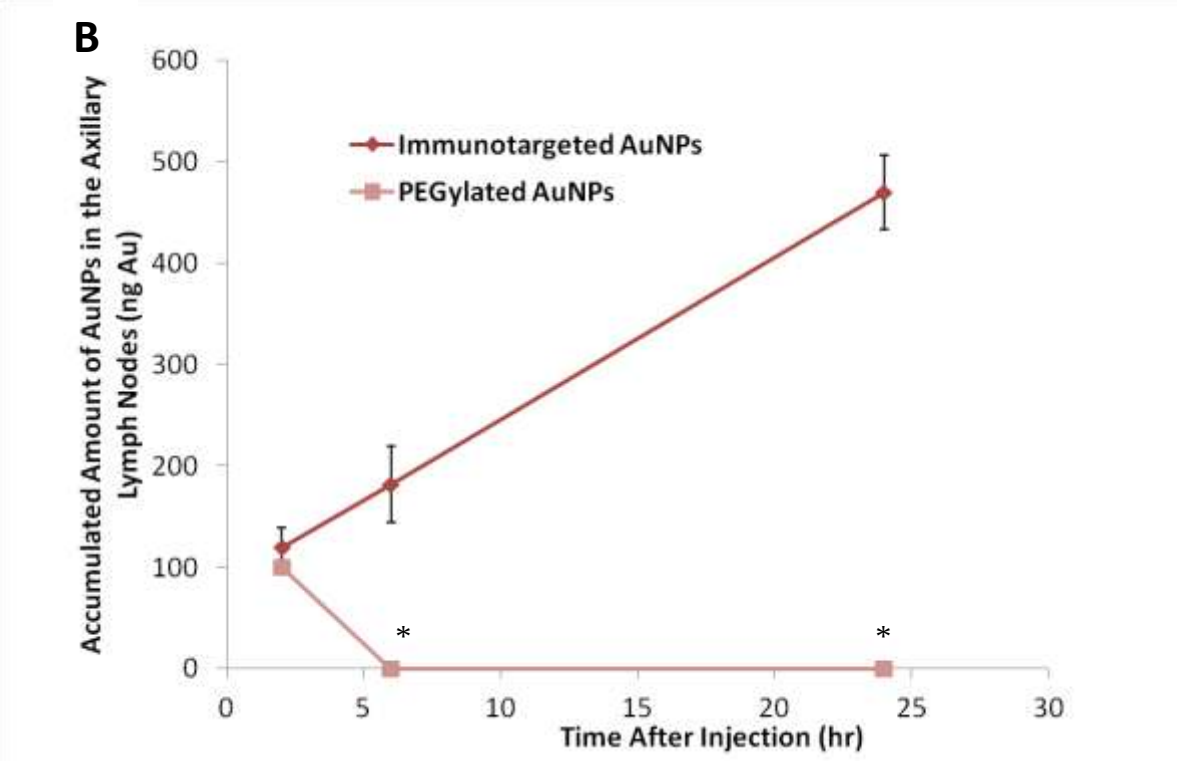

* Below the detection limit (~10 ng)

Figure 6. ICP-MS quantitative data of gold in (A) popliteal lymph nodes (B) axillary lymph nodes, comparing anti-CD45 conjugated gold nanoparticles and PEGylated gold nanoparticles at different time points post-injection.